Photocatalytic decomposition of ethylene using He plasma induced nano-TiO_2

Shin Kajita

Institute of Materials and Systems for Sustainability, Nagoya University, Nagoya 464-8603, Japan

Yudai Tomita

Graduate School of Engineering, Nagoya University, Nagoya 464-8603, Japan

Eriko Yasunaga

Graduate School of Agricultural and Life Sciences, The University of Tokyo

Tomoko Yoshida

The OCU Advanced Research Institute for Natural Science and Technology, Sumiyosi, Osaka, 555-8585, Japan

Kazuya Miyaguchi, Hirohiko Tanaka, and Noriyasu Ohno

Graduate School of Engineering, Nagoya University, Nagoya 464-8603, Japan *

(Dated: June 3, 2019)

Abstract

Ethylene decomposition via photocatalytic reaction using ultra-violet light was performed using oxidized titanium (Ti) sheet and/or thin film samples fabricated by helium (He) plasmas treatments. We prepared nanostructured Ti samples formed by He plasma irradiation and additional thin film deposited samples using radio frequency magnetron sputtering. The samples prepared in this study had a slightly lower photocatalytic activity compared to the thin film deposited on tungsten nanostructure samples previously reported; the anatase formation was solely identified on Ti sheet samples in the present study and is hopeful for further improvement of photocatalytic activity of plasma treated titania.

PACS numbers:

*Electronic address: kajita.shin@nagoya-u.jp

Ethylene (C_2H_4) is the plant hormone that promotes fruit ripening, aging, and a wide range of other plant processes [1]. Ethylene has been used in postharvest technologies such as inductions of flower and sprout [2]; on the other hand, it can induce harmful reactions for postharvest fruit and vegetable, because it accelerates aging and shortens the preserved duration in shelf even in a small amount [3]. One of the promising solutions is likely decomposition of ethylene via catalytic/photocatalytic materials [3, 4] in addition to adsorption [5], oxidation [6], decomposition using nonthermal plasma [7], and usages of environment level actions such as ventilation, controlled atmosphere storage, and modified atmosphere packaging [3].

Among photocatalysts using ultra-violet (UV) light, titania (TiO_2) is regarded as the most attractive and efficient material with its stable properties and low cost [3]. However, because the recombination of photogenerated charges limits the photocatalytic performance, photocatalysts with higher performance are required to be developed. One of the way to enhance photocatalytic performances is usages of micro- and nano-materials [8, 9], and plasmas can be used for fabrications of such fine materials.

In addition to reactive plasmas, which have been widely used as a nanofabrication tool for silicon and carbon based materials [10, 11], potential of usage of helium (He) plasmas to metallic materials has been identified in this ten years. The He irradiation effect of nanostructuring metal surfaces was first identified on tungsten (W) [12] and later on other metals including molybdenum [13], titanium (Ti) [14], tantalum, iron [15], rhenium, iridium [16, 17], rhodium, and ruthenium [18]. Although formation mechanism has yet to be fully understood, it is recognized that formed He nano-bubbles by He ion bombardment play important roles for the growth of fiberform nanostructures [19]. Photocatalytic activity of He plasma induced nanostructures have been investigated on (partially) oxidized W [20–23], vanadium [24], niobium [25], iron [26]and titanium [27].

In this study, we use helium (He) plasmas to induce morphology changes in micro- and nano-meter scales, and photocatalytic performance of those fabricated materials to degrade ethylene is measured. Recently, it was shown that TiO_2 thin layer formed on He induced nanostructured W increased the decomposition of ethylene via photocatalytic decomposition [27]. In this study, nanostructures were formed directly on Ti surfaces by irradiating He plasmas to Ti.

He plasma irradiations were conducted in the linear plasma device NAGDIS-II, and the

details of the setup in the device can be found elsewhere [18]. A 0.2-mm-thick Ti sheet (99.5%, Nilaco Co.) with a size of 25×25 mm was installed in the downstream of the NAGDIS-II device and exposed to the He plasma. The sample was installed in a water cooling stage. The incident ion energy was controlled by negative biasing of the sample, and the temperature was controlled by the heat flux from the plasma and the heat resistance to the cooling stage.

Figure 1(a) shows a scanning electron microscope (SEM) micrograph of Ti sample exposed to the He plasma under the following irradiation condition: the incident ion energy of 75 eV, the surface temperature of 800 K, and the He fluence of 8×10^{25} m^{-2}. Although the structures did not have a complete fiberform, fine rough structures, the size of which was less than 1 μm, was formed on the surface. Previous systematic He plasma irradiation to Ti revealed that pinholes, nano-cones, and microstructures were mainly able to be formed easily on the surface [14]; fiberform nanostructures were formed on the surface at the fluence higher than 10^{26} m^{-2}. Since the temperature and the incident ion energy in Fig. 1(a) were almost consistent with those in cases where fiberform nanostructures were grown, finer fiberform nanostructure could have been grown when the fluence was higher.

After the He plasma irradiation, 100-nm-thick Ti thin film was deposited using a radio frequency magnetron sputtering device (SHIMADZU, HSR-522) on the nanostructured surface. Figure 1(b-d) shows SEM micrographs of the thin film deposited surfaces oxidized at the air atmosphere at 673, 773, and 873 K, respectively. The oxidization was performed using a furnace for two hours. With increasing the oxidization temperature, the roughness increased typically from 200-300 nm at 673 K to 400-500 nm at 873 K.

In this study, we used (i) pristine Ti sheet without plasma exposure (Ti_{pr}), (ii) Ti sheet exposed to the He plasma (Ti_N), and (iii) 100-nm-thick Ti thin film deposited on Ti sheet exposed to the He plasma (Ti_{NTF}). Here, subscripts 'pr', 'N', and 'NTF' came from pristine, nanostructures, and thin film deposited on nanostructures, respectively. In addition, we compare the performance of the three kinds of samples to (iv) 100-nm-thick Ti thin film deposited on W sheet after the exposure to the He plasma (W_{NTF}). The oxidization temperature was shown in parentheses after the sample name such as $Ti_{pr}(673)$ or $Ti_{NTF}(873)$. The oxidation time was fixed at two hours for all the samples in this study.

Raman spectra of the prepared samples were taken using a laser Raman spectrometer (Jasco, NRS-1000) using a laser at the wavelength of 532 nm. The measurement depth

was ∼500 nm with the spatial resolution of several μm. Titania exists as two polymorphs, the rutile and anatase, and natase transforms to rutile at elevated temperatures [28]. It is possible to descern from Raman spectra whether rutile and/or anatase are formed. The rutile is stable and anatase is an metastable. Because they have different properties, they exhibits different photocatalytic performances. In Fig. 2(a-c), Raman spectra of samples oxidized at 673, 773, and 873 K, respectively, are presented. It is noted that the spectra intensities altered significantly by position for the samples oxidized at 673 and 773 K. As a typical example, two spectra on $Ti_N(673)$ sample at different positions are shown in Fig. 2(a). It is shown that the intensities are quite different from position to position, indicating that the sample was not oxidized uniformly. The non-uniformity was not only found on Ti_N samples, but also on Ti_{pr} and Ti_{NTF} samples as well at the oxidization temperatures of 673 and 773 K. When the sample was oxidized at 673 K, anatase peaks [29] were found mainly, while rutile peaks dominated at 873 K. Anatase and rutile were mixed together at 773 K. It is known in general that anatase has a better photocatalytic performance than rutile [30].

Photocatalytic decomposition of ethylene was performed at room temperature using a quartz glass reactor which has a total volume of 210 ml. The prepared samples were irradiated with UV light from a 300 W xenon lamp via a cold mirror. A small amount of ethylene gas was introduced to the reactor to reach the concentration of ∼50 ppm. We waited for an hour after the injection of ethylene to be uniformly distributed in the reactor and started UV light irradiation. The concentration of C_2H_4 (C, ppm) was measured using a gas chromatograph (Shimadzu, GC-2014).

Figure 3(a) show time evolutions of the ethylene concentration normalized to the initial value, C/C_0, for $Ti_{pr}(673)$, $Ti_N(673)$, and $Ti_{NTF}(673)$, in addition to no sample case. In all the three cases, the concentration decreased monotonically with the irradiation time. The best performance was identified on Ti_{NTF} and followed by Ti_N. Figure 3(b) summarize the decomposition rate of ethylene in the initial one hour. On Ti_{pr} and Ti_N samples, the decomposition rate decreased with increasing the oxidized temperature. This was probably because active anatase was changed to rutile with increasing the oxidation temperature. At all the temperatures, Ti_N samples had a higher performance than that of Ti_{pr} samples. On the other hand, the performance decreased significantly from 673 to 773 K on Ti_{NTF} sample and improved when the oxidation temperature increased to 873 K.

Previously, on Ti thin film deposited samples on nanostructured W formed He plasma

irradiation, photocatalytic performance increased with the oxidation temperature of up to 873 K, suggesting that the crystallinity gradually changed together with the formation of rutile [27]. Thus, one possibility to improve the photocatalytic performance from 773 to 873 K is due to the fact that the crystallinity of the thin coating layer was improved when the temperature increased to 873 K, while anatase was changed to lower performance rutile. We have tried to confirm the above speculation using X-ray diffraction (XRD); however, clear signal was not be able to be obtained, probably because the film is too thin to eliminate the bulk property. It is our future work to investigate the influence of the crystalinity of deposited thin films.

Comparing the photocatalytic performance of the samples using Ti bulk to that of W_{NTF}, which was investigated in detail previously [27], the best performance was obtained on $W_{NTF}(873)$. It is noted that Tomita *et al.* optimized the oxidization temperature and thin film thickness [27], and the best performance of W_{NTF} samples was obtained at the oxidization temperature of 873 K, the oxidization time of 2 hours, and the Ti film thickness of 100 nm. In Fig. 3(b), the performance of $W_{NTF}(873)$ is also shown. The performance of $W_{NTF}(873)$ is slightly better than that of $Ti_{NTF}(673)$. This is probably because W surface exposed to the He plasma had much finer nanostructures and greater surface area compared to Ti_{NTF} sample surfaces. On $W_{NTF}(873)$, recycle experiment of photocatalytic decomposition of ethylene was performed (Fig. 4). The performance was kept for five recycling times, suggesting that the surface was not degraded by the photocatalytic reactions.

Although the best performance was obtained on W_{NTF} sample, a possibility of Ti substrate case is in the fact that anatase was formed on the surface at the oxidization temperature of 673 K, which was not identified on W_{NTF} sample cases. If the difference in the photocatalytic performance between the $Ti_{NTF}(673)$ and $Ti_{NTF}(873)$ was caused by the crystallinity of thin film, it is expected that the performance can be significantly on Ti_{NTF} samples if the crystallinity is improved even at the oxdization temperature of 673 K. It is of interests to try forming better film samples by optimizing the surface temperature by heating the sample during the deposition or inserting annealing process before oxidation in vacuum.

This work was supported in part by a Fund for the Promotion of Joint International

Research 17KK0132 from the Japan Society for the Promotion of Science (JSPS).

---

[1] K. Golden *et al.*: Asian Journal of Biological Sciences **7** (2014) 135.

[2] A. A. Kader, *Postharvest technology of horticultural crops* (University of California Agriculture and Natural Resources, 2002), Vol. 3311.

[3] N. Keller, M.-N. Ducamp, D. Robert and V. Keller: Chemical Reviews **113** (2013) 5029, pMID: 23590210.

[4] S. S. Satter, T. Yokoya, J. Hirayama, K. Nakajima and A. Fukuoka: ACS Sustainable Chemistry & Engineering **6** (2018) 11480.

[5] K. Abe and A. E. Watada: Journal of Food Science **56** (1991) 1589.

[6] R. Wills and M. Warton: Journal of the american society for horticultural science **129** (2004) 433.

[7] K. Takaki, J. Nishimura, S. Koide, K. Takahashi and T. Uchino: IEEE Transactions on Plasma Science **43** (2015) 3476.

[8] M. Haruta: CATALYSIS TODAY **36** (1997) 153.

[9] S. Kwon, M. Fan, A. T. Cooper and H. Yang: Critical Reviews in Environmental Science and Technology **38** (2008) 197.

[10] K. Ostrikov: Rev. Mod. Phys. **77** (2005) 489.

[11] V. M. Donnelly and A. Kornblit: Journal of Vacuum Science & Technology A **31** (2013) 050825.

[12] S. Takamura, N. Ohno, D. Nishijima, and S. Kajita: Plasma and Fusion Research **1** (2006) 051.

[13] S. Takamura: Plasma Fusion Res. **9** (2014) 1405131.

[14] S. Kajita, D. Kitaoka, N. Ohno, R. Yoshihara, N. Yoshida and T. Yoshida: Applied Surface Science **303** (2014) 438.

[15] S. Kajita, T. Ishida, N. Ohno, D. Hwangbo and T. Yoshida: Sci. Rep. **6** (2016) 30380.

[16] Y. Ueda, N. Yamashita, K. Omori, H. Lee, K. Ibano and A. Ito: Journal of Nuclear Materials **511** (2018) 605 .

[17] S. Takamura and Y. Uesugi: Applied Surface Science **356** (2015) 888.

[18] S. Kajita, T. Nojima, Y. Tomita, N. Ohno, H. Tanaka, N. Yoshida, M. Yajima, T. Akiyama,

M. Tokitani and T. Yagi: Surface and Coatings Technology **340** (2018) 86.

[19] S. Kajita, N. Yoshida, N. Ohno and Y. Tsuji: New Journal of Physics **17** (2015) 043038.

[20] S. Kajita, T. Yoshida, D. Kitaoka, R. Etoh, M. Yajima, N. Ohno, H. Yoshida, N. Yoshida and Y. Terao: Journal of Applied Physics **113** (2013) 134301.

[21] M. de Respinis, G. De Temmerman, I. Tanyeli, M. C. van de Sanden, R. P. Doerner, M. J. Baldwin and R. van de Krol: ACS Applied Materials & Interfaces **5** (2013) 7621.

[22] K. Komori, T. Yoshida, T. Nomoto, M. Yamamoto, C. Tsukada, S. Yagi, M. Yajima, S. Kajita and N. Ohno: Nuclear Instruments and Methods in Physics Research Section B: Beam Interactions with Materials and Atoms **365, Part A** (2015) 35.

[23] K. Komori, T. Yoshida, S. Yagi, H. Yoshida, M. Yajima, S. Kajita and N. Ohno: e-J. Surf. Sci. Nanotech. **12** (2014) 343.

[24] S. Kajita, T. Yoshida, N. Ohno, Y. Ichino and N. Yoshida: Journal of Physics D: Applied Physics **51** (2018) 215201.

[25] S. Kajita, F. Mimuro, T. Yoshida, N. Ohno and N. Yoshida: ChemPhysChem **19** (2018) 3237.

[26] R. Sinha, I. Tanyeli, R. Lavrijsen, M. van de Sanden and A. Bieberle-Hutter: Electrochimica Acta **258** (2017) 709.

[27] Y. Tomita, S. Kajita, E. Yasunaga, T. Yoshida, N. Ohno and H. Tanaka: Japanese Journal of Applied Physics **58** (2019) SEEG01.

[28] D. A. H. Hanaor and C. C. Sorrell: Journal of Materials Science **46** (2011) 855.

[29] U. Balachandran and N. Eror: Journal of Solid State Chemistry **42** (1982) 276.

[30] T. Luttrell, S. Halpegamage, J. Tao, A. Kramer, E. Sutter and M. Batzill: Scientific reports **4** (2014) 4043.

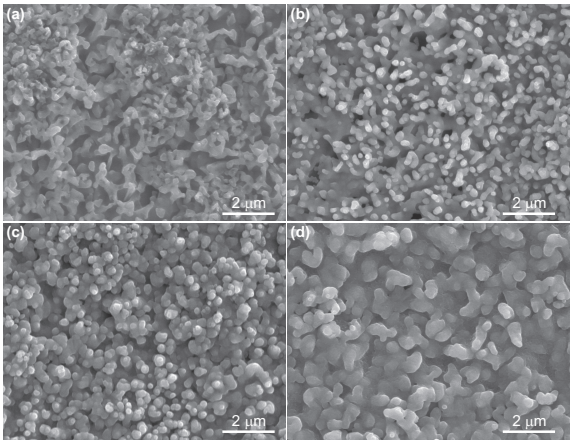

FIG. 1: SEM micrographs of (a) Ti sample exposed to He plasma, and (b-d) thin film deposited sample on Ti exposed to He plasma oxidized at 673, 773 and 873 K, respectively.

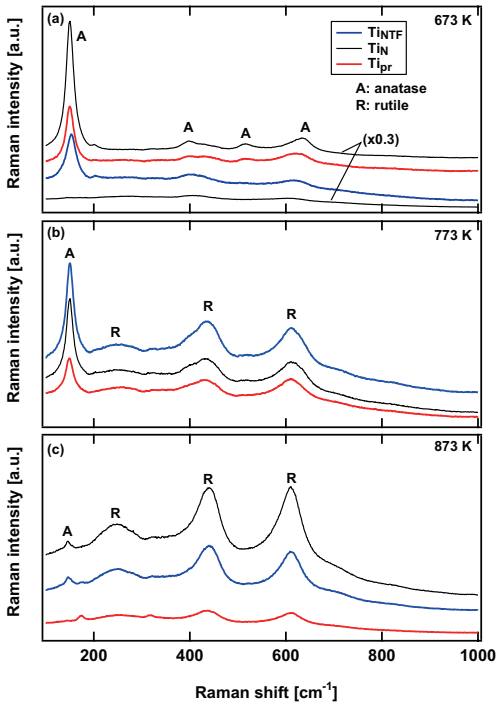

FIG. 2: Raman spectra of samples (Ti_{pr}, Ti_N, Ti_{NTF}) oxidized at (a) 673, (b) 773, and (c) 873 K are presented.

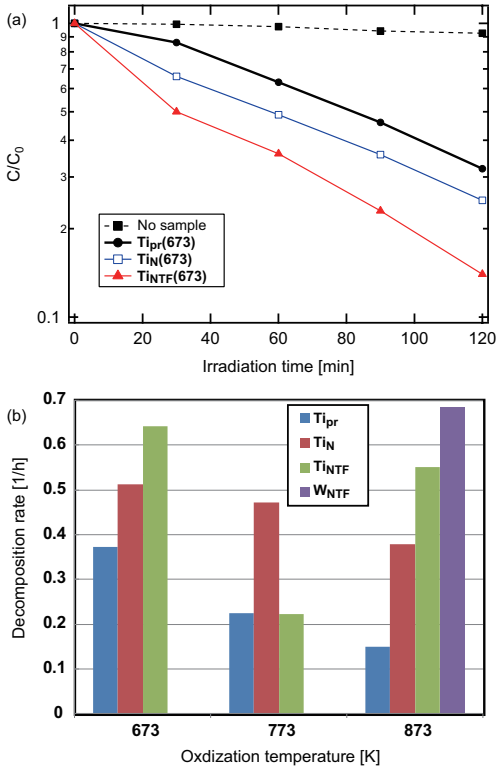

FIG. 3: (a) Time evolutions of C/C_0 for $\mathrm{Ti_{pr}}(673)$, $\mathrm{Ti_N}(673)$, and $\mathrm{Ti_{NTF}}(673)$, in addition to no sample case and (b) a summary about the decomposition rate of ethylene in the initial one hour for $\mathrm{Ti_{pr}}$, $\mathrm{Ti_N}$, and $\mathrm{Ti_{NTF}}$ samples. In (b), the performance of $\mathrm{W_{NTF}}(873)$ [27] is also shown.

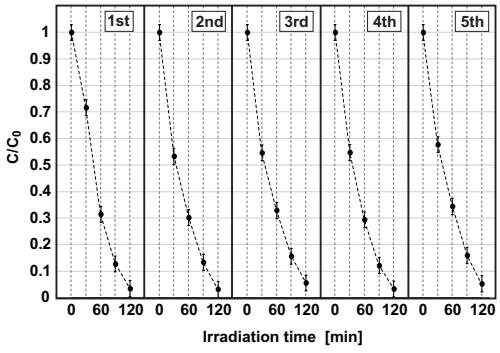

FIG. 4: Recycle experiments performance of $\mathrm{W_{NTF}}(873)$.